1D Hydro-geomechanical Modelling of Pore Pressure on an Active Convergent Margin: East Coast Basin, New Zealand

Erika E. Calderon Medina[1], Joshua Obradors-Prats[2,3], Andrew C. Aplin[1], Stuart J. Jones[1], Mohamed Rouainia[2], Anthony J. Crook[3].

[1] Department of Earth Sciences, Durham University

[2] School of Engineering, Newcastle University

[3] Three Cliffs Geomechanical Analysis Ltd

*Copy of the manuscript accepted for The Offshore Technology Conference, Houston, USA, 2023

Abstract

This study aims to understand the causes of anomalous pore fluid pressures within sedimentary sequences of an active tectonic basin through well log analysis, pressure data evaluation and thermo-hydro-geomechanical modelling. The study focuses on the East Coast Basin (ECB), New Zealand, an active convergent margin, where anomalously high pore pressures have been encountered in deep-water systems at burial depths as shallow as 200 m.

A regional investigation including analysis of the Cretaceous to Holocene tectono-stratigraphy and diagenetic histories of the ECB, was combined with seismic and well log interpretation to understand the structural and sedimentation history of the ECB, and thus the main factors that were likely to contribute to overpressure generation/dissipation and porosity loss. 1D hydro-geomechanical models were then built to undertake a parametric study to investigate the effect on porosity and pore pressure evolution of different sedimentation and erosion rates, hiatus periods, different erosion thicknesses, and tectonic compression. The parametric models show that high overpressures can be preserved during rapid erosion events due to the relatively small timeframe for pore pressure dissipation, depending on sediment permeability. Furthermore, only recent erosion events are relevant to the present-day overpressure. In addition, high levels of tectonic compression (12.5 %) applied in recent events can produce both high pore pressure values and significant porosity reduction if the sedimentary column was undercompacted prior to the tectonic compression.

Learnings from the parametric studies were used as a starting point to understand controls on the pore pressure and porosity in the Opoutama-1 well, located on the onshore area of the ECB. Results from the Opoutama-1 well show that the high pore pressure registered at shallow depths (< 1 km) in this well is significantly driven by tectonic compression as a result of high subduction rates (presently 48 mm/yr). Disequilibrium compaction also contributed to overpressure generation due to high sedimentation rates (up to ~3000 m/Ma). However, much of the disequilibrium compaction-related overpressure was dissipated during uplift, hiatus, and erosion. Where overpressure is preserved, it is related to thick (up to 1 km) mudstone packages deposited during the Cretaceous to Holocene, thin low permeable layers of limestones deposited during the Miocene to Pliocene and marl intervals with high content of smectite.

1 Introduction

High overpressures at shallow depths in the East Coast Basin (ECB) are a drilling hazard and increase the costs and risks for hydrocarbon exploration, exploitation, and potentially CO_2 and hydrogen storage. The accurate identification of the mechanisms which contribute to the overpressure could mitigate uncertainties and reduce costs and risks.

The basin has a complex Cretaceous to present-day geological history, with multiple periods of erosion, tectonic events and changes in sedimentation and erosion rates; this means that it is difficult to evaluate potentially multiple controls on present-day pore pressure, and also the evolution of pore pressure through time. Modelling offers a way to explore the potential importance of the various parameters that influence pore pressure development and dissipation. The aim of this study is to apply 1D hydro-geomechanical modelling to identify and quantify the overpressure mechanisms, with a step-by-step explanation of how multiple models were used to investigate the quantitative influence of sedimentation and erosion rates, erosive events, hiatus periods, low permeability layers and tectonic compression, and to highlight the variables which have the most impact.

1.1 General Setting

The research area of this study is the ECB (Figure 1), an active basin where the Pacific Plate subducts beneath the Australian Plate (Field et al., 1997; Ballance, 1975).

The ECB is gas and oil-prone tested with more than one hundred wells drilled onshore and offshore. The main reservoirs are sandstones deposited in deep-water systems affected by deep currents (contourites) (Ballance, 2017; Bailey et al., 2021); the seals are thick intervals of mudstones (e.g., Pindari Formation), a smectite-rich calcareous mudstone (e.g., Wanstead Formation) and thin intervals of low porosity carbonates (e.g., limestones of the Tahaenui, Kiakia and Kauhauroa Formations) (Field et al., 1997). The main source rocks are shales of the Palaeocene and Late Cretaceous (Waipawa and Whangai Fm.) (Rogers et al., 1999). The structures are anticlines related to thrust and strike-slip faults with a stratigraphic component (Figure 1).

Reservoirs in this basin are sandstones and limestones located at different depths and formations. Porosity reduction has been attributed to pore-filling authigenic calcite and compactional deformation (Watters,

1990). Nevertheless, core samples taken in different wells of different formations show a range of porosities (e.g., Torlesse Formation 15 %, Rere Formation 17.8 %, Tunanui Formation 29.5 %, Poha Formation 26.2 %) (Figure 2) (Martin, 1995).

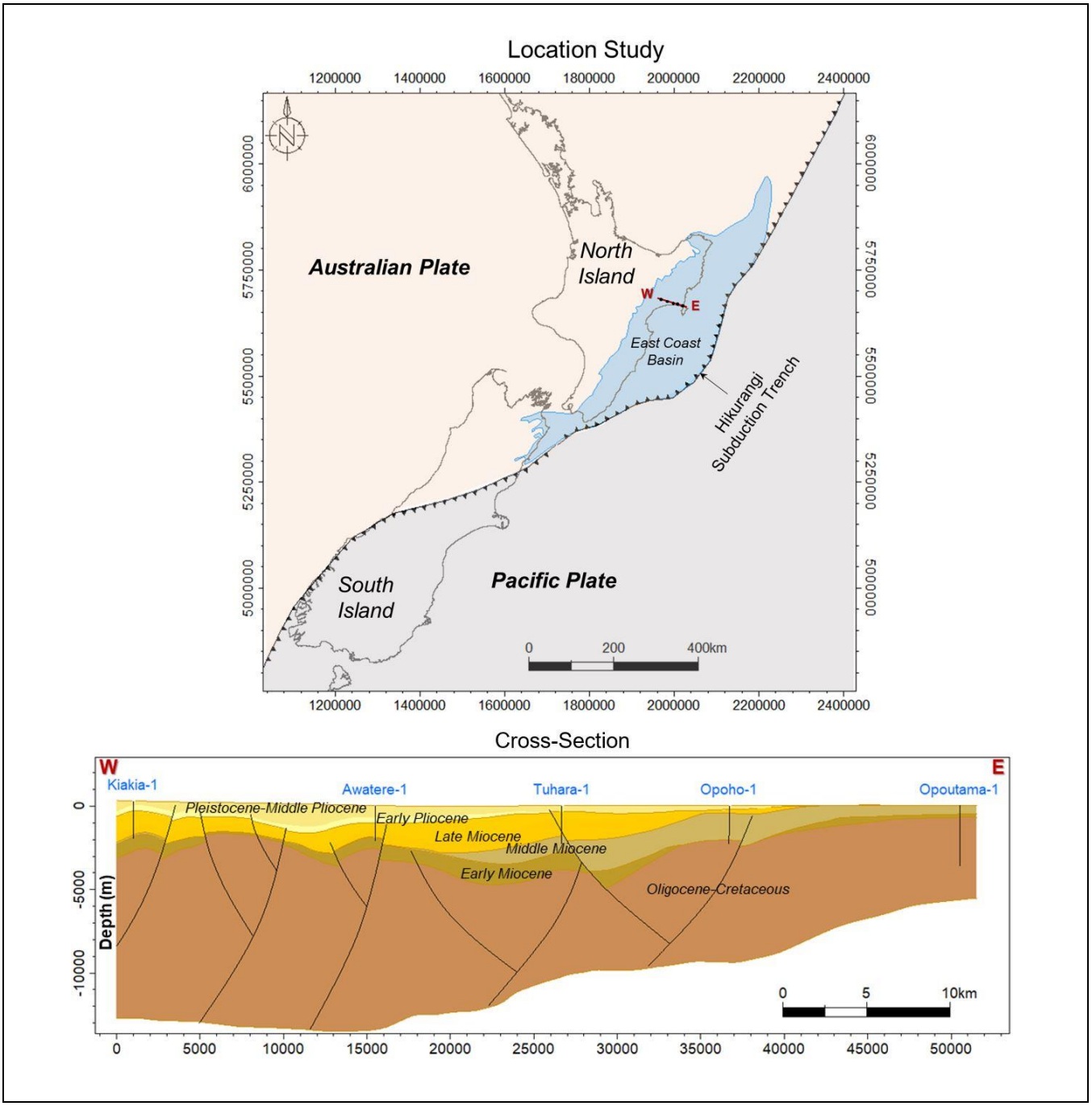

Figure 1.- Location map and cross-section of the research area.

The geothermal gradient calculated in this basin is between 23 and 24°C/km (Field et al., 1997; Funnell et al., 1999) with a surface temperature of 24 °C and the hydrostatic gradient is 0.433 (0.002985 MPa/m) (Watson, 1962) to 0.45 psi/ft (0.0031026 MPa/m) (Brown, 1960).

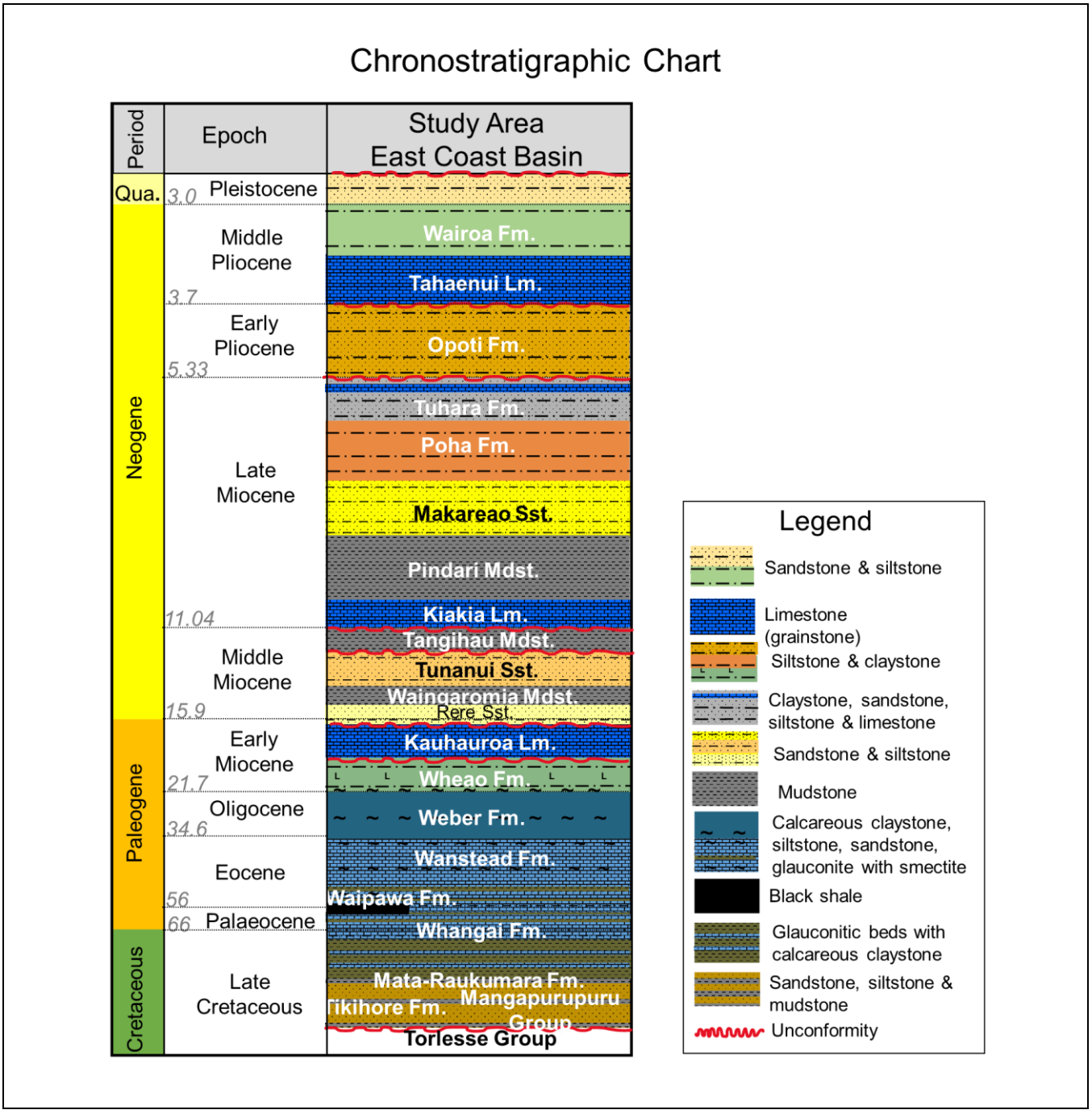

Figure 2.- Chronostratigraphic chart with the main formations encountered in the ECB research area. Source ECB well reports and Raine et al., (2015).

2 Data and Methods

Data for the East Coast Basin were obtained through the New Zealand Petroleum and Mine Online Exploration Database (NZPAM), the New Zealand Crown Research Institute (GNS) and the General Bathymetric Chart of the Oceans (GEBCO).

Primary data for this study are from seismic surveys and well reports. The data consist of twenty-two well log sets (GR, RHOB, DT and resistivity), twenty wells with mud weight values, nine wells with RFT, MDT or DST, ninety-eight well reports, one 3D seismic survey and approximately four hundred 2D seismic lines in time with two 2D seismic lines in depth. Results are presented in metres (m), and kilometres (km) for distances, thickness and depths, mega Pascal (MPa) for pore pressure, squared meters (m^2) for permeabilities and fraction or percentage (%) for porosity.

The software used were Petrel (version 2019 to 2022.2), Petromod (version 2021.2) and ParaGeo (version 3.9.3).

It should be noted that the numbering adopted to identify the models in this manuscript is not always consecutive because only the relevant results from all the cases simulated are presented.

3 Pore Pressure Interpretation

3.1 Well Logs

Even though the ECB is an active basin, normal standard compaction trends were obtained from sonic and density logs generated using Wyllie's (1956) and Athy's (1930) equations (1 and 2). Interpretation of the results, in terms of normal compaction trends and pore pressure, is not straightforward due to the complex geological evolution of this basin. To calibrate these trends, an eroded interval (ei), which varies in each location, was calculated qualitatively, and used in the analytical equations. The eroded thickness started from 0 m (no erosion) to 2,000 m, and the best fit was selected.

1: $$\Delta t_{NC} = \Delta \mathrm{t}_{ma} + (\Delta \mathrm{t}_{ml} - \Delta \mathrm{t}_{ma}) * e^{c*(-Z-ei)}$$

2: $$\rho_{NC} = \rho_{ma} + (\rho_{ml} - \rho_{ma}) * e^{c*(-Z-ei)}$$

Where Δt_{NC} is the transit time for normal compaction, Δt_{ma} is the matrix transit time (67us/ft), Δt_{ml} is the mudline transit time (seabed) (188 us/ft), z is the depth below sea level (m), c is the compaction coefficient (0.0005 m^{-1}) after Hansen (1996) and Tingay et al., (2009), ei is the eroded interval, ρ_{NC} is the density of the normal compaction, ρ_{ma} is the matrix density (2.67 gr/cm^3) and ρ_{ml} is the density at the mudline (1.73 g/cm^3) (Couzens-Schultz and Azbel, 2014).

Normal compaction trends for mudstones were also obtained with Athy's (1930) equation, a method used previously by Funnell et al., (1996) to identify eroded sections in New Zealand basins; this approach calculates the porosity at normal compaction and subtracts a value which represents the thickness eroded. In this research the missing section has been represented by (ei) (equations 3 and 4). This equation is typically used only for the mudstone sections, but it can be applied for other lithologies.

3: $$\emptyset_{mudstones\&\,carbonates} = \emptyset_{mud} * e^{c*(-z-ei)}$$

4: $$\emptyset_{sandstones} = \emptyset_{sst} * e^{c*(-z-ei)}$$

In equations 3 and 4 $\emptyset_{mudstones}$ is the porosity of mudstones, $\emptyset_{sandstones}$ is the porosity of sandstones, $\emptyset_{mud}$ and $\emptyset_{sst}$ is the porosity at mudline (e.g., 0.54 for mudstones and 0.45 for sandstones), (z) is the depth in metres below sea level and c is the compaction constant (e.g., 0.0005 for mudstones and 0.000333 for sandstones). The initial porosities and compaction values in these equations were determined using New Zealand data (Funnell et al., 1996).

This method can be used to estimate the eroded thickness during the last erosive event. However, the effect of pore pressure, effective stress, and other erosive intervals (e.g., regional, and local unconformities interpreted on seismic and wells) along the sedimentary column cannot be determined with analytical equations, therefore geomechanical modelling was used to investigate the evolution of pore pressure.

3.2 Pressure Data

The data analysed included nine drill stem tests (DST), one repeat formation tester (RFT), one modular formation dynamics tester (MDT) and twenty wells with mud weights. In this basin, pressure data are scarce and have been taken in sandstones. Nevertheless, it has been noticed that pore pressure starts increasing below thick intervals of mudstone, thin layers of limestone and formations with smectite. From the assessment it is observed that overpressure is not related to a depth, region or formation, which was also recognised by Darby and Funnell (2001).

4 Geomechanical Modelling

To illustrate the effect of sedimentation, erosion, hiatus and tectonic compression on pore pressure and porosity evolution, 1D models based on a simplified geological history were created. These models facilitate the understanding of the effect of different parameters on pore pressure evolution, initially considering the effect of rapid sedimentation at different rates, and then incorporating additional geological events to examine the roles of additional overpressure generation mechanisms, and the role of pressure dissipation. Similar models have been used to understand sediment behaviour and to calibrate parameters such as porosity-permeability and compaction curves (e.g., Darby and Ellis, 2001; Obradors-Prats et al., 2017a; Obradors-Prats et al., 2017b). The second part of this research was to apply the findings to the Opoutama-1 well, located on the onshore area of the ECB, creating calibrated 1D column models that aim to capture the stratigraphic and geological history of the basin, to better understand the potential of a range of geological processes on pore pressure development in the region.

4.1 Definition of Column Models

The initial model geometry comprises a 20 m width, 300 m length single lithology mudstone, upon which fourteen additional, 300 m thick layers are deposited. The normal compaction curve is based on Schneider's model, (1996). The porosity-permeability curve used in the parametric models (Parametric Models in Figure 3) is a modification of Kozeny-Carmen's standard mudstone (K-C Shale in Figure 3) which depends on porosity and pore throat size of the lithology.

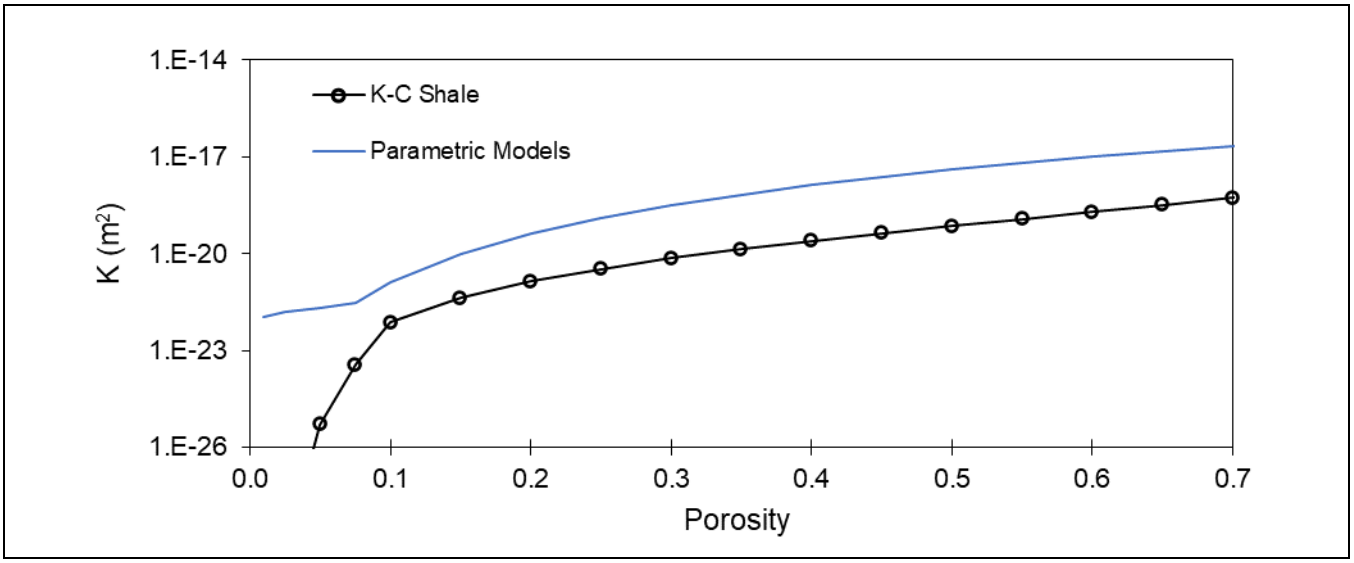

Figure 3.- Kozeny-Carmen's standard mudstone curve and a modified curve used in all the parametric models for mudstone-lithologies. The minimum value used for permeability was 1.E-22 m^2.

4.1.1 Sedimentation Rates

The sedimentation rates considered in the parametric study are summarised in Table 1 and are based on studies performed in the ECB and other basins around the world (e.g., Audet, 1996; Swarbrick and Hillis, 1999; Swarbrick et al., 2002; Darby and Funnell, 2001; Neef, 1992).

Table 1.- Sedimentation rates model inputs.

Model	Sed. rate (m/Ma)	Sed. duration per layer (Ma)
2	200	1.5
3	500	0.6
4	1,000	0.3
1	2,000	0.15
36	3,000	0.1

The model results show that the faster the sedimentation rate, the higher the predicted pore fluid pressure as the system becomes increasingly undrained. For instance, at 3 km a pore pressure of 44 MPa is observed when the sedimentation rate is 3,000 m/Ma, in comparison to 32 MPa at the same depth with a sedimentation rate of 200 m/Ma. Porosity is preserved due to the effect of overpressure in reducing the vertical effective stress; for example, at 3 km a porosity of 0.29 is observed with a sedimentation rate of 3,000 m/Ma, and a porosity of 0.18 at the same depth with a sedimentation rate of 200 m/Ma. If the porosity is preserved due to under compaction, the thickness is preserved with a thickness difference of 200 m between the cases with the slowest and the fastest sedimentation rates.

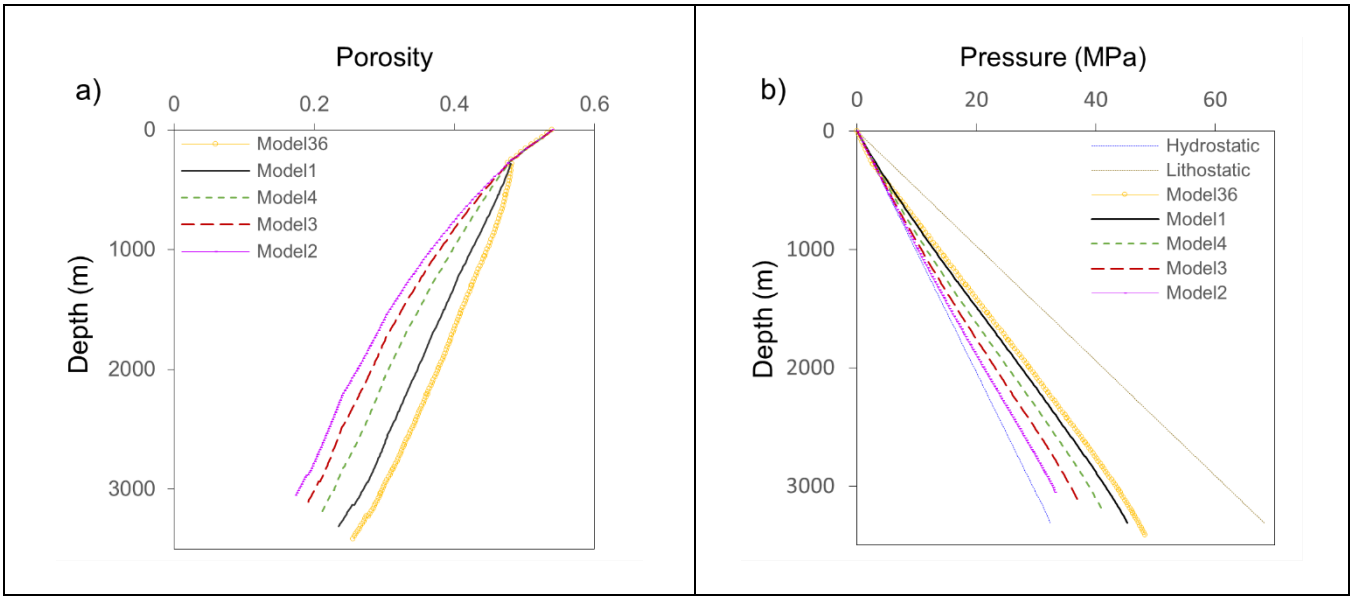

Figure 4.- a) porosity vs depth plot with five cases showing different sedimentation rates (model2 = 200 m/Ma, model3 = 500 m/Ma, model4 = 1,000 m/Ma, model1 = 2,000 m/Ma and model36 = 3,000 m/Ma) and b) pore pressure vs depth plot showing how pore pressure increases as sedimentation rates increase. A water gradient (hydrostatic) of 0.00105 MPa/m and a lithostatic gradient of 0.0226 MPa/m were used.

4.1.2 Eroded Thickness

In this section, the effect of eroded thickness on porosity and pore pressure evolution was evaluated. The models factor in a deposition phase at a constant sedimentation rate of 2,000 m/Ma (fifteen layers were deposited of 300 m each) followed by an erosion event with different eroded thicknesses (different number of eroded layers) (Table 2).

Table 2.- Models with one to four eroded layers with the same erosion time.

Model	Sed. rate (m/Ma)	Sed. time per layer (Ma)	Number of eroded layers	Total erosion time (Ma)
40	2,000	0.15	4	0.15
39	2,000	0.15	3	0.15
38	2,000	0.15	2	0.15
8	2,000	0.15	1	0.15

During erosion there are three factors which contribute to the evolution of pore pressure and porosity. This includes the fluid flow during erosion which leads to overpressure dissipation; the exhumation of sediments and the reduction in the mechanical load associated with the weight of the eroded sediments.

Figure 5 shows that there is a noticeable pressure difference between model 1 (a model with no erosion) and the remaining models, which is related to the fluid flow (overpressure dissipation). The slight pressure differences between models 8, 38, 39 and 40 are because all models were constructed using the same erosion time frame (0.15 Ma) and therefore the overpressure dissipation due to fluid flow is similar in all the models.

The pressure changes can therefore be attributed to the differences in the mechanical load reduction and flow pathway lengths in each model as a result of the different eroded thicknesses.

The porosity figure also shows a greater difference between models 1 and 8 which is related to the exhumation of previously deeper buried, more highly compacted sediments. The effective stress increases due to overpressure dissipation and porosity reduces due to mechanical compaction.

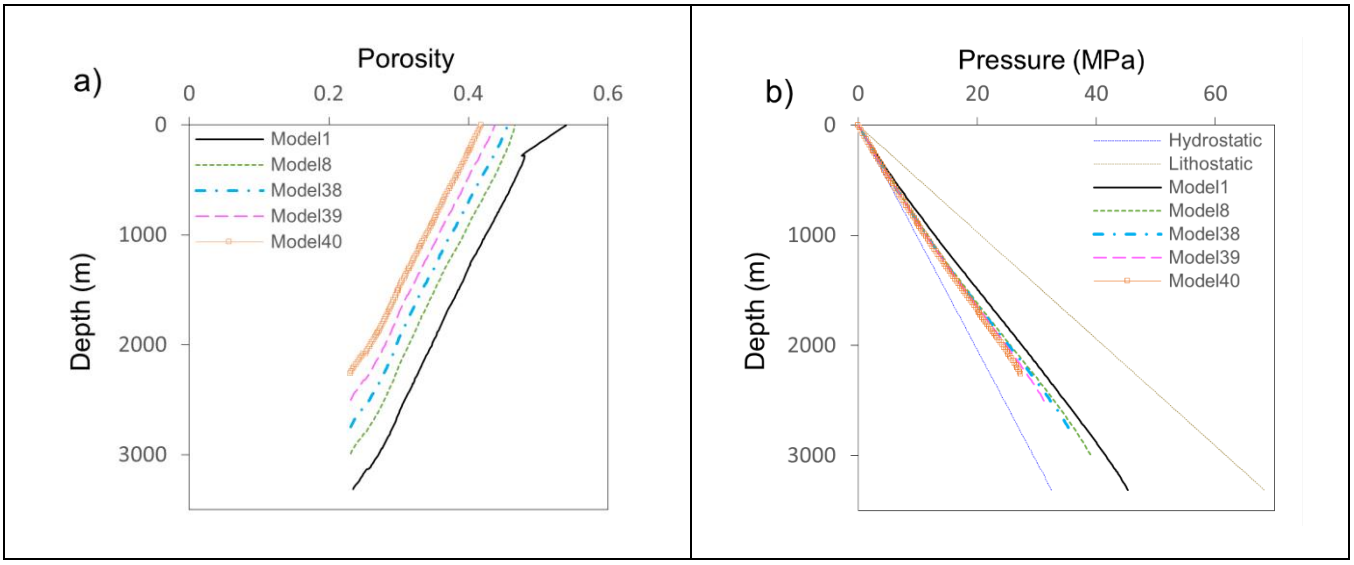

Figure 5.- a) porosity vs depth plot with the five models where model40 = 4 eroded layers, model39 = 3 eroded layers, model38 = 2 eroded layers, model8 = 1 eroded layer and model1 does not have any eroded layer, and b) fluid pore pressue vs depth plot showing the reduction of pore pressure due to erossion of the models 8, 38, 39, and 40. Model1 has the complete sedimentary column, without erosion events.

4.1.3 Effect of Erosion Rates and Sedimentation Rates

The effects of different erosion rates were assessed with models 8 to 11. These models consider an initial phase of sedimentation with a constant sedimentation rate of 2,000 m/Ma (fifteen layers were deposited of 300 m each) followed by an erosion event where one layer is eroded at different erosion rates. The input is presented in Table 3 and the results are shown in Figure 6a and Figure 6b.

Table 3.- These models test different erosion rates in one layer.

Model	Sed. rate (m/Ma)	Sed. time per layer (Ma)	Number of eroded layers	Total erosion time (Ma)
8	2,000	0.15	1	0.15
9	2,000	0.15	1	0.3
10	2,000	0.15	1	0.45

11	2,000	0.15	1	0.6

A second set of models (model-1H, model-3H and model-5H) was used to investigate the effect of sedimentation subsequent to erosion in porosity and pressure. After the initial sedimentation phase, in which 4,500 m of sediments (fifteen layers of 300 m each) were deposited with a constant sedimentation rate of 2,000 m/Ma, five layers were eroded (removed thickness 1,500 m) with a constant erosion rate of 2,000 m/Ma). This is followed by another sedimentation phase with a constant sedimentation rate of 2,000 m/Ma in which the models consider different thicknesses of deposited sediments (model-1H = 300 m, model-3H = 900 m, and model-5H = 1,500 m). Model inputs are presented in Table 4 and the results are shown in Figure 6c and Figure 6d.

Table 4.- Main inputs of the models that investigated high and low sedimentation and erosion rates with different additional sedimentation post-erosion.

Model	Sed. rate (m/Ma)	Sed. time per layer (Ma)	Number of eroded layers	Total erosion time (Ma)	New sed. layers	Sed. rate (m/Ma)
1H	2,000	0.15	5	0.15	1	2,000
3H	2,000	0.15	5	0.15	3	2,000
5H	2,000	0.15	5	0.15	5	2,000

In models 1H, 3H and 5H (Figures 6c and 6d) the erosion of five layers (1,500 m) led to a reduction in the overpressure generated during the sedimentation phase, and the exhumation of the deep, more highly compacted sedimentary column to shallower levels.

During the next sedimentation phase a discontinuity is observed in the porosity plot model 1-H at 300 m between the first sedimentation phase and the subsequent one, as the exhumed sediments are over-

consolidated. Therefore, these sediments will not develop any further plastic compaction until the previous maximum stress is overcome, leaving the possibility of only elastic porosity reduction.

Consequently, the potential overpressure generation during sedimentation after erosion is low in comparison to the overpressure generated during the first sedimentation. It is noticed that model 5-H, which has reached the same thickness previously eroded (1,500 m), predicts lower porosity and lower pressure than model 1 (case with no erosion). This is a result of the overpressure dissipation due to fluid flow during erosion and during subsequent sedimentation above over-consolidated sediments.

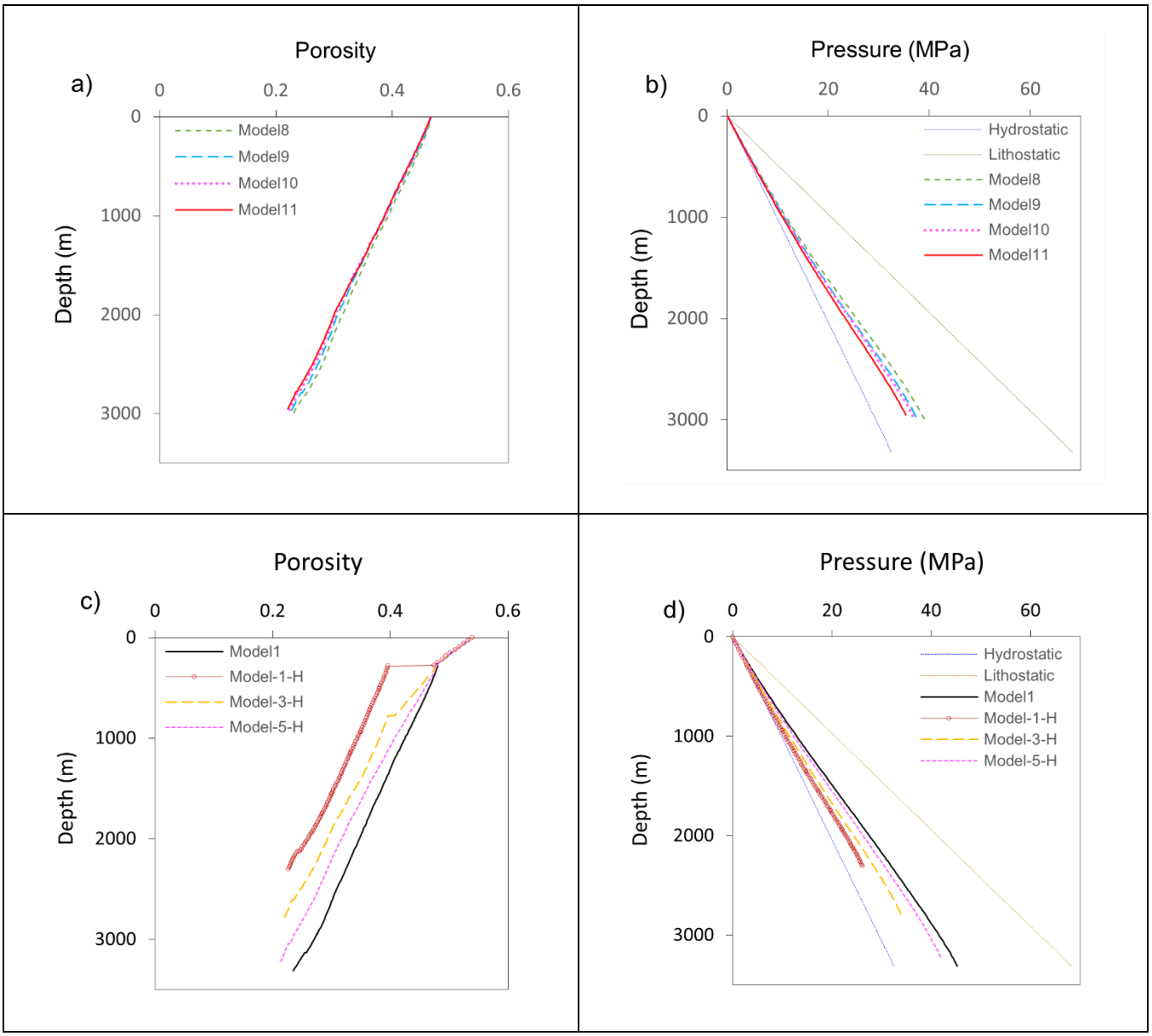

Figure 6.- a) porosity and b) pore pressure show results of models testing the influence of erosion rate of the most recently deposited sediments. c) porosity and d) pore pressure show results of models testing the influence of different additional sedimentation thickness following the erosion of part of the previously deposited sedimentary sequence. Model1 has the same sedimentation rate (2,000 m/Ma) but without erosion or addional sedimentation, and is shown for comparisson.

4.1.4 Hiatus

These models investigated pore pressure dissipation during different hiatus periods that follow the sedimentation of fifteen layers of 300 m, each at a sedimentation rate of 500 m/Ma. Model inputs are presented in Table 5 and results are shown in Figures 7a and 7b.

Table 5.- Main inputs of models that investigated the effect of hiatus on porosity and pore pressure.

Model	Sed. rate (m/Ma)	Sed. time per layer (Ma)	Number of hiatus events	Hiatus time (Ma)
21	500	0.6	1	0.6
22	500	0.6	1	1.2
23	500	0.6	1	1.8
24	500	0.6	1	2.4

In the absence of a very low permeability sealing layer or any other overpressure mechanism acting on the sediments, previously generated overpressure dissipates due to fluid flow during a hiatus period. The longer the hiatus period, the larger the overpressure dissipation and consequently the lower the predicted overpressure and porosities.

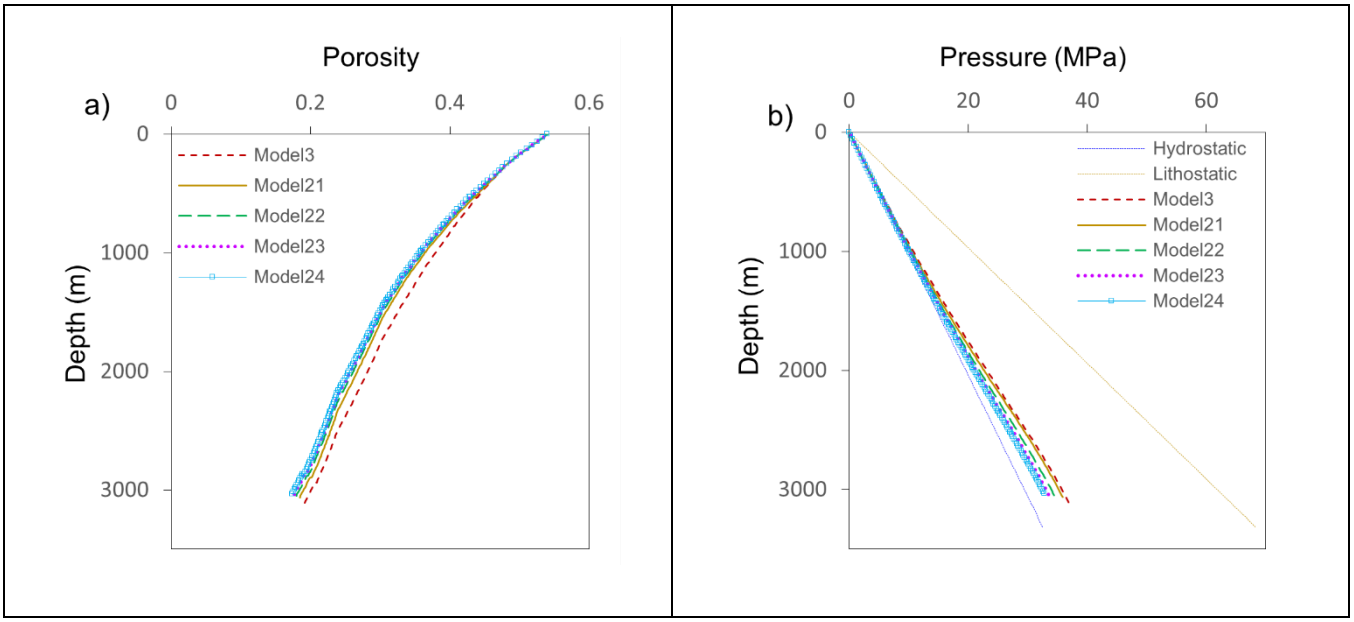

Figure 7.- a) porosity vs depth plot with models that represent different hiatus periods and b) pore pressure vs depth showing how pore pressure is dissipated through time without any further sedimentation. Model3, which has the same sedimentation rate (500 m/Ma) but without a hiatus, is used to compare porosity and pore pressure.

4.1.5 Tectonic Compression with Constant Shortening

These models assessed disequilibrium compaction and tectonic compression together. An analysis of the shortening values described in previous studies in the ECB (e.g., Nicol et al., 2002; Bailleul et al., 2013; Reyners, 2013), shows that these values represent displacements of faults and deformation obtained from restorations on seismic sections. However, those restorations neglected tectonic compaction.

Studies such as Butler and Paton, (2010) and Dalton et al., (2015) have compared restored displacements in the extensional and contractional domains on gravitational thrust belt systems, where the recovered displacements in the extensional domain are larger than the displacements recovered in the compressional structures, attributing the missing strain component to tectonic compaction (shortening values from 5% to 12.6%).

Due to the lack of well-constrained tectonic strain estimates for the ECB, shortening values between 5 and 12.6 % were adopted to investigate its effect on pore pressure, porosity, and effective stresses.

Models 12 to 15 have a constant shortening of 5% occurring during the deposition of the last one to four layers with a constant sedimentation rate of 500 m/Ma (Table 6). The shortening distance depends on the width of the models and the shortening percentage; models in this study are 20 m wide.

Table 6.- Main inputs of models that investigated the effect of shortening applied during the deposition of the last 1-4 deposited layers.

Model	Sed. rate (m/Ma)	Sed. time per layer (Ma)	Number of layers deposited during tectonic compression	Shortening % applied	Tectonic compression time (Ma) per layer
12	500	0.6	1	5	0.6
13	500	0.6	2	5	0.6
14	500	0.6	3	5	0.6
15	500	0.6	4	5	0.6

Modelled pore pressures increase with shortening rate; if the shortening is only applied during the last depositional event, tectonic-induced overpressure can only dissipate in this period (Model12). If the same amount of shortening is applied during the last four deposition events, the time for pore pressure dissipation is four times greater (Model15). Another contributing factor is that for models starting from 15 (four layers) to 12 (one layer) there is an increasing thickness of sediment pre-dating the onset of tectonic compaction and consequently a larger volume of pore fluid accommodating the tectonic load and a longer dissipation pathway from the bottom of the column to the top surface (Figure 8b). Additionally, there is a tectonic-induced porosity reduction ranging from 1 to 1.5 units depending on the depth (Figure 8a).

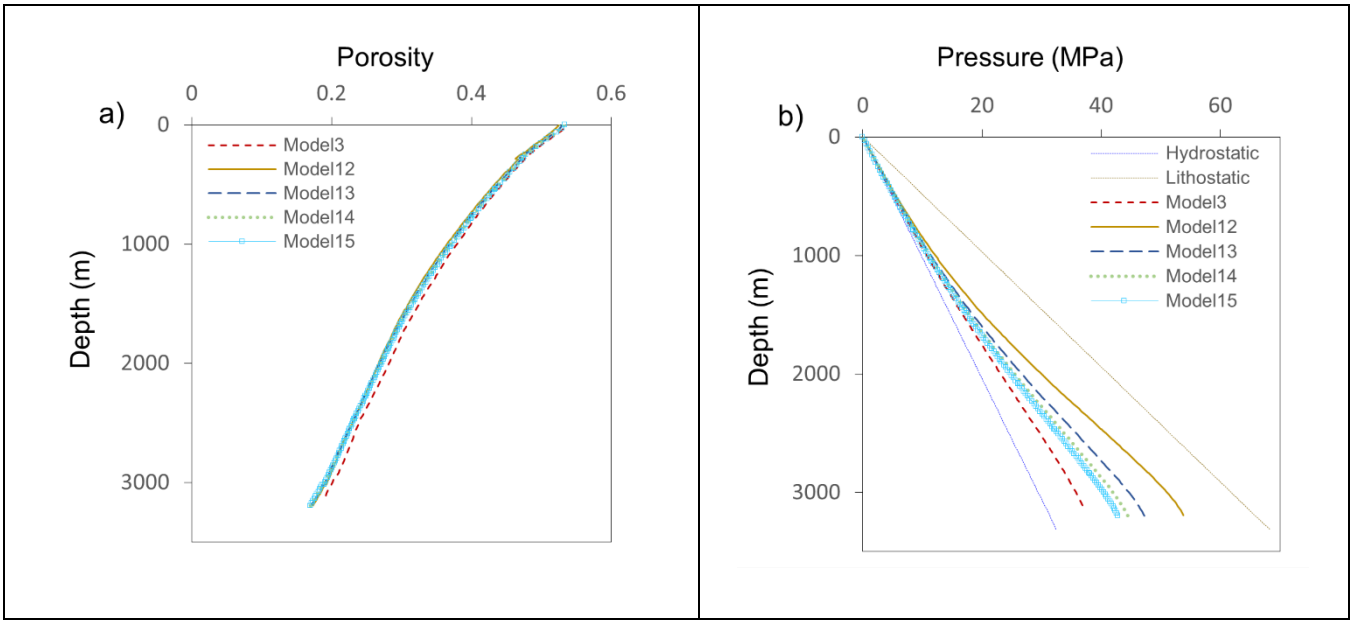

Figure 8.- a) porosity vs depth plot showing the reduction of porosity due to tectonic compression applied for different lengths of time; b) pore pressure vs depth showing that the time period over which tectonic compression is applied influences the pore pressure throughout the whole depositional sequence. The greatest effect is when tectonic compression is restricted to the latest depositional event as shown with Model12. See Table 6 for model inputs.

4.1.6 Tectonic Compression with Different Shortening

In this section was evaluated disequilibrium compaction and the effect of different shortening percentages applied only during the last depositional event. To represent tectonic compression, shortening distance or shortening percentages are used. These models have a sedimentation rate of 500 m/Ma with a shortening percentage between 5 and 12.5 % (Table 7).

Table 7.- Main inputs of models that investigated different amounts of tectonic compression (shortening distance), applied during the deposition of the last deposited sediment layer.

Model	Sed. rate (m/Ma)	Sed. time per layer (Ma)	Number of layers deposited during tectonic compression	Shortening % applied	Tectonic compression time (Ma) per layer.	Total shortening distance (m)
16	500	0.6	1	1	0.6	0.2
12	500	0.6	1	5	0.6	1
17	500	0.6	1	10	0.6	2

18	500	0.6	1	12.5	0.6	2.5

The pore pressure was directly related to the shortening distance: the greater the shortening distance the higher the pore pressure. The maximum shortening applied during this test was 12.5 % (Model18) which is consistent with the maximum estimated value due to tectonic compaction (e.g., Butler and Paton, 2010; Dalton et al., 2015). Greater levels of tectonic compression can result in greater porosity reduction. However, it depends on the compaction of the lithology (e.g., in models 16, 12, 17, 18 at 1,000 m depth a reduction of 2.5 units was obtained during modelling (Figure 9a)).

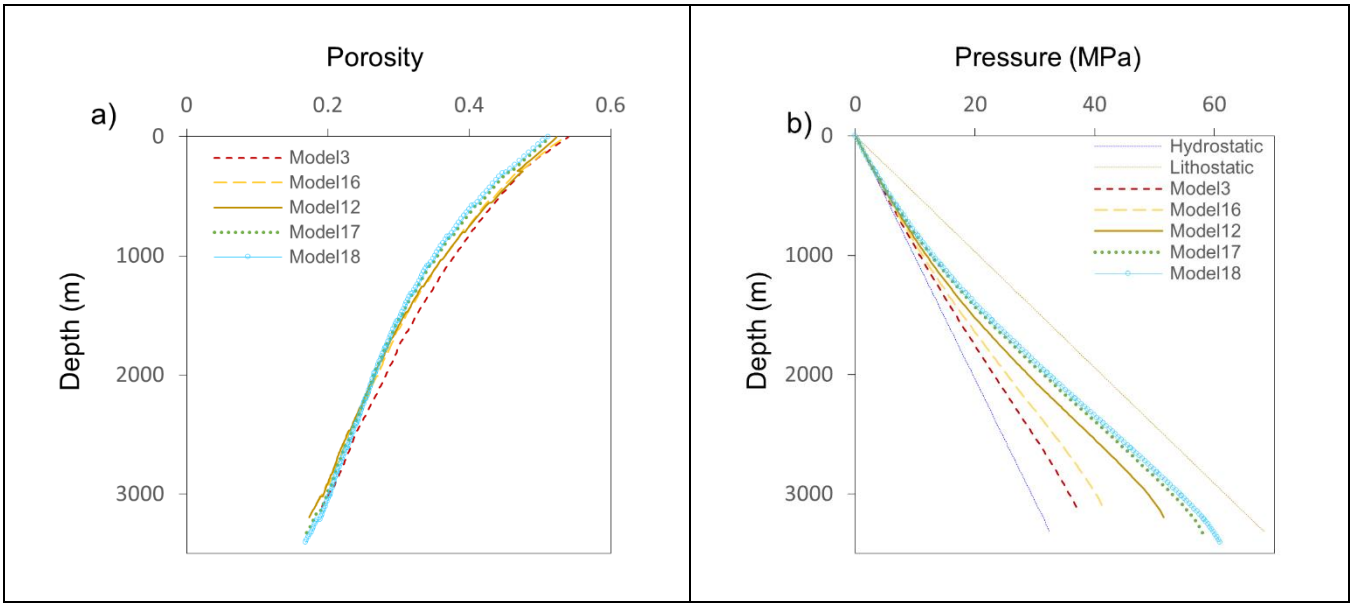

Figure 9.- a) porosity vs depth showing the porosity reduction as a result of tectonic compression applied during the deposition of the most recent sediment layer; b) pore pressure vs depth showing that increased shortening during the deposition of the most recent sediment layer results in increased pore pressure. Model3 has the same sedimentation rate (500 m/Ma) without tectonic compression, and it is shown for comparison.

4.2 Opoutama-1 Column Model

The insights obtained from the single material models enabled the identification of the parameters that could play a role in overpressure generation in geologically complex regions such as the ECB; this included eroded sediment thickness, hiatus and timing and extent of tectonic shortening percentage. The findings were applied on the Opoutama-1 well, located in the ECB, onshore New Zealand. The total depth

of this well is ~3,657 m and penetrated sediments range from the Middle Miocene (~11.04 Ma) to the Cretaceous (~72.081 Ma). Two regional unconformities, identified in seismic data, well logs and well reports were considered in the geomechanical models: one during the Early Miocene and a second which eroded Pleistocene, Middle Pliocene, and Early Pliocene sediments.

In the ECB, seals to petroleum accumulations have been identified to be thick intervals of mudstones for the Late Miocene, the Eocene Wanstead Formation, and thin tight intervals of limestones for the Early Miocene to Middle Pliocene (Figure 2). However, in this well only the Wanstead Formation was registered during drilling; the other intervals were either not deposited or were eroded, so that the focus here is on the Wanstead Formation and any other intervals with low permeability that allow the generation of overpressure. In general, in the ECB this formation has a variable thickness (~100 to 300 m) and consists of fine-grained calcareous sediments with intercalations of mudstone, siltstone, and sandy mudstones (Field et al., 1997). The amount of smectite is variable with an increase up to ~41 % of $CaCO_3$ in certain areas (Lillie, 1953; Haskell, 2005) while in others this formation has more intercalations of bentonite (indicative of extensive volcanism during this period) (J. A. R. 1985; Simpson et al., 1993).

For the Opoutama-1 well models, five compaction and porosity-permeability curves, which represent five lithologies were created. These curves are modification of the standard curves obtained from Schneider et al., (1996), and Kozeny-Carmen (Figure 10).

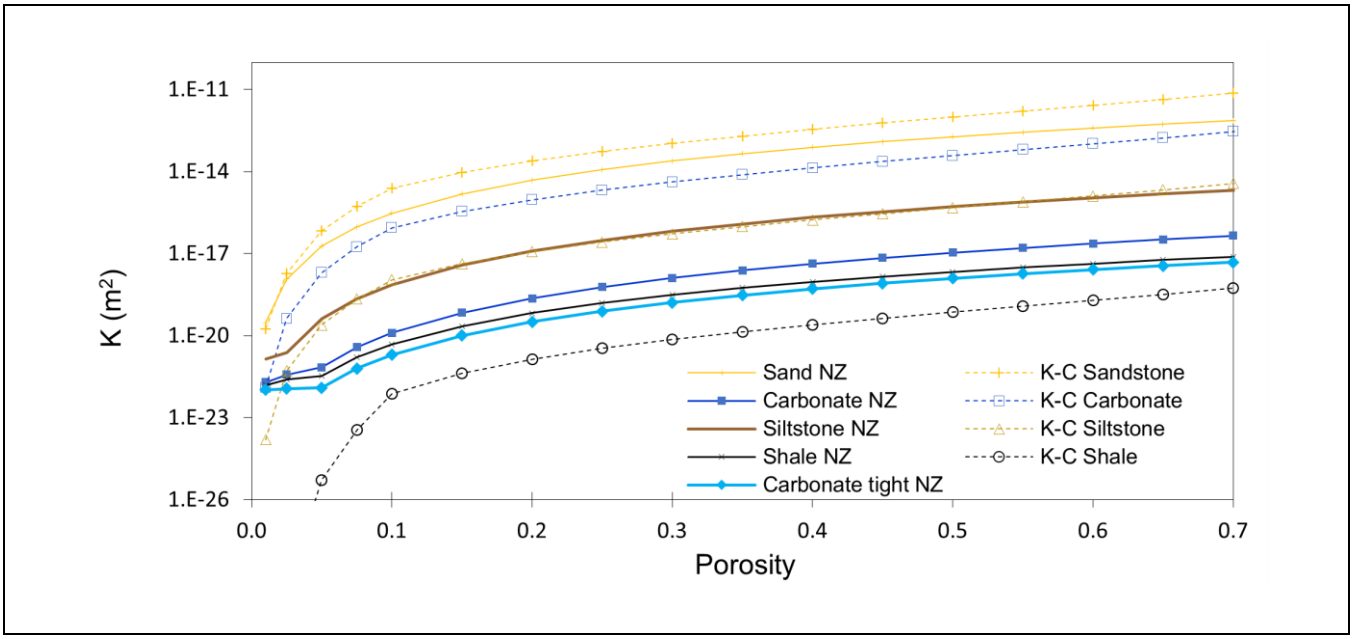

Figure 10.- Porosity permeability relationships adopted for the different lithologies in the New Zealand models. Typical Kozeny-Carmen curves for different lithologies as defined in Hantschel and Kauerauf, (2009) are provided for reference. The minimum permeability used in the models was 1.E-22 m².

4.2.1 Opoutama-1 Column Model Settings

Due to the large uncertainty in the geological history, multiple models with different assumptions relative to sedimentation, erosion thicknesses, hiatus timescales and tectonic compression were built (Table 8). The 1D models built in this section represent the most significant events identified during this research. As a reference porosity curve (in blue), pore pressure test (DST in purple), and pore pressure from mud weights (in light blue) are presented in Figure 11a and Figure 11c; these data were used to calibrate models.

High porosities (up to 0.34) occur in the Wanstead Formation at depths between ~1,170 to ~1,370 m (Figure 11a and Figure 11c). At the same depth in the pore pressure plot, pore pressure from mud weights increases from 12 to 18 MPa. According to well reports, this interval contains ~80 % montmorillonite (smectite) with low organic content and with a possible fracture system (NZ Aquitaine Petroleum Ltd., 1967).

To investigate the effect of the Wanstead Formation on pore pressure the porosity-permeability and compaction curves were changed to a material with low petrophysical properties (Model_Opoutama-7T and 5T) (Figure 11c and Figure 11d). Such curves were obtained from the calibration of the tight intervals

evaluated in other wells. The permeability reduction in comparison to models (Opoutama-1T, 3T, 4T and 6T) is approximately three orders of magnitude (2.5 E-19 to 3.7 E-21 m^2 at ~1,170 m depth).

Table 8.- Scenarios investigated in the Opoutama-1 well.

Model	Disequilibrium Compaction (sedimentation, hiatus, and erosion)	Disequilibrium Compaction (sedimentation, hiatus, and erosion) + Tectonic Compression
Opoutama-1 (1T)	Yes, no hiatus	No
Opoutama-1 (3T)	Yes	No
Opoutama-1 (4T)	Yes	8 %
Opoutama-1 (6T)	Yes	12.5 %
Opoutama-1 (5T)	Yes, plus one tight layer (Wanstead Formation) (highlighted in dark blue in Figure 11c)	8 %
Opoutama-1 (7T)	Yes, plus one tight layer (Wanstead Formation) (highlighted in dark blue in Figure 11c)	No

The models are ~3.6 km length and 20 m width and are represented by five lithologies: mudstone, siltstone, carbonate marls, carbonate tight and sand. The present-day thickness and porosity of each lithology were derived from the well log analysis. Then, with assumed depositional porosities, the depositional thicknesses and porosity were calculated to input to the models. All the models performed for this well have the same configuration until the Late Miocene (blue cells in Table 10) which include sedimentation, tectonic and erosion events.

Model_Opoutama-1T considers sedimentation, after the Late Miocene during the events labelled as 9a, 9b, 10a, 10b, 11a and 11b. This model finishes with an erosive event (erosion2), which considers the removal of 5,025 m of sediments, which is the sum of the uncompacted thicknesses of events 8a to 11b in Table 10. Results are shown in Figure 11.

Models_Opoutama-3T, 4T, 5T, 6T and 7T consider that sediments corresponding to events 9a to 11b were not deposited (hiatus) as opposed to being deposited and later eroded. These models also finish with an

erosive event (erosion2), which in this case erodes 1,711 m of sediments (corresponding to sediments deposited during events 8a and 8b in Table 10) (Figure 11).

Table 9.- 1D Column models depositional and erosional settings.

Period	Total time (Ma)	Event	Lithology	Init. porosity	Init. thickness (m)
Pleistocene	3	erosion2			
		11b	Siltstone	0.50	128
		11a	Shale	0.54	139
Middle Pliocene	0.7	10b	Shale	0.54	739
		10a	Siltstone	0.50	680
Early Pliocene	1.63	9b	Shale	0.54	848
		9a	Siltstone	0.50	780
Late Miocene	5.71	8b	Shale	0.54	891
		8a	Siltstone	0.50	820
Middle Miocene	4.86	7	Sandstone	0.45	342
		6	Shale	0.54	443
Early Miocene	5.8	erosion1			
		5a	Shale	0.54	413
		5	Shale	0.54	282
Oligocene	12.9	4	Carbonate	0.43	328
Eocene	21.4	3	Carbonate	0.43	639
Paleocene	10	2	Shale	0.50	1236
Cretaceous	6.1	1	Shale	0.54	2629

As the uncertainty of sedimentation and erosion rates, the thickness eroded, periods of non-deposition, and the amount of tectonic compaction is high, numerous models were investigated. From these only the models which agree with the geology of the area and present a reasonable calibration of measured data are presented. For instance, models that investigated different deposited and later removed thicknesses from the Late Miocene to the Pleistocene are not presented as the results showed that at the well location a small sedimentary column was deposited and eroded.

Results show that disequilibrium compaction (sedimentation hiatus and erosion) is not sufficient to generate the overpressure encountered in this well (Models_Opoutama-1T, 3T and 7T) (Figure 11b and Figure 11d). On the other hand, tectonic compression (Models_Opoutama-4T, 5T and 6T) has a significant impact on the pore pressure, requiring a shortening of 12.5 % (Model_Opoutama-6T) to fit the available DST measurements. Such shortening corresponds to the maximum value estimated in previous studies (e.g., Butler and Paton, 2010; Dalton et al., 2015). However, it is noted that due to the simplification of the geology considered in the models (i.e., no faults or structures are considered) even with these two mechanisms (disequilibrium compaction and tectonic compression) the results could not be calibrated to fit all the pressure estimations available from the mud weight.

Model_Opoutama-1T shows lower porosity values compared to results predicted by models 3T, 4T, 5T, 6T and 7T, which considered more sediments deposited (9a, 9b, 10a, 10b, 11a, 11b) and later eroded (event erosion2); this could indicate that at the well location sediments were not deposited during the Pleistocene, Middle Pliocene, and Early Pliocene.

In Model_Opoutama-7T high porosities are preserved due to the high overpressure generated during sedimentation. Below the tight interval (~1,170 to ~1,370 m) starting around 1,500 m depth, the overpressure is constant with a pressure gradient parallel to the hydrostatic. This is an effect due to the porosity-permeability curves adopted in the models and the large porosity generated; the resulting permeability is high enough to enable overpressure equilibrium below the seal over geological time (Figure 11d).

Model_Opoutama-5T accounts for the same depositional, hiatus and erosional configuration as Model_Opoutama-7T, but with the addition of tectonic compression. In this scenario porosities further decreased, and pore pressure almost reached the lithostatic. In this scenario pore pressure gradient is sub-parallel to the lithostatic in mudstones located below the low-permeable interval (~1,170 to ~1,370 m) (Figure 11c).

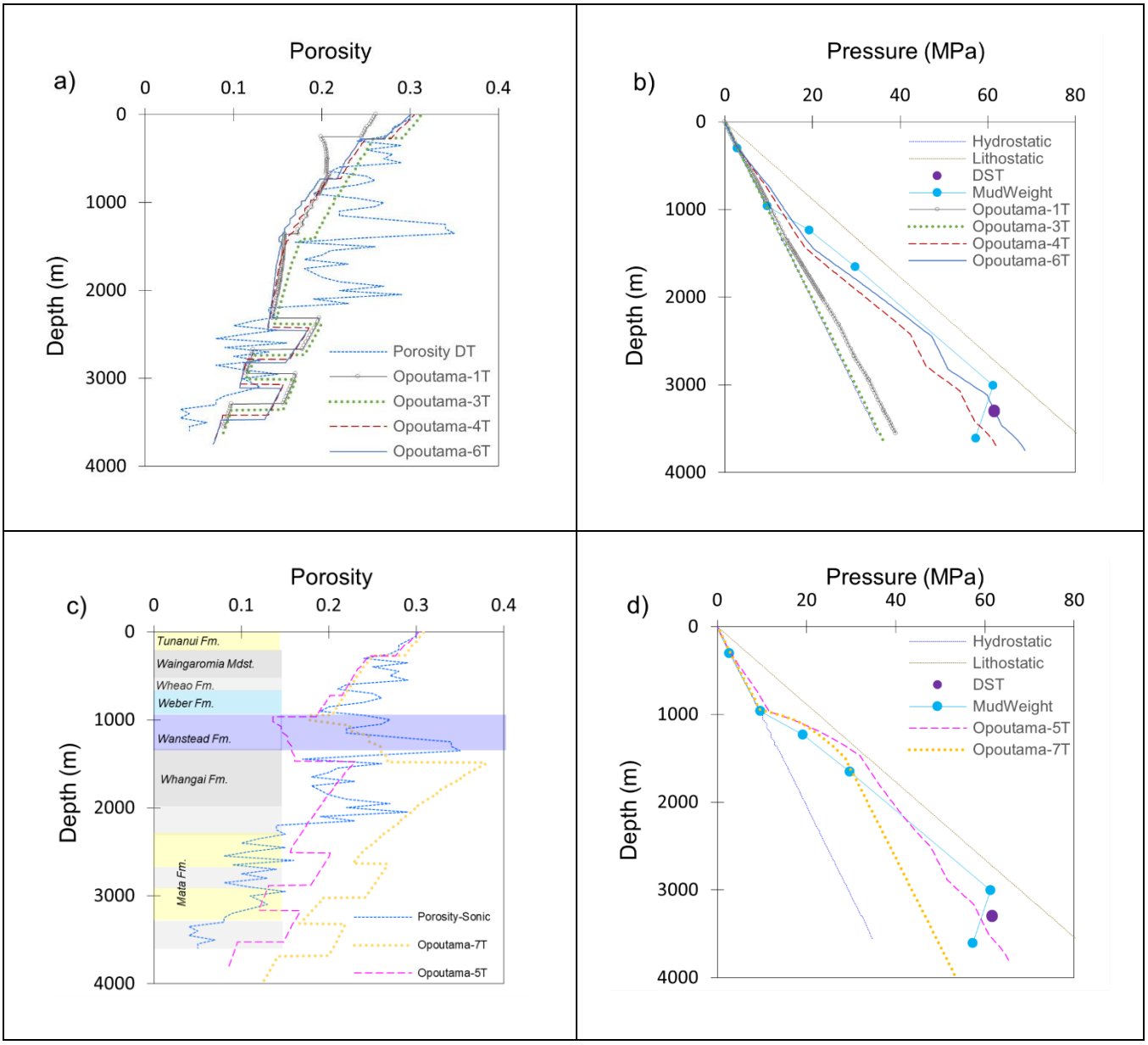

Figure 11.- Summary of the scenarios investigated in the Opoutama-1 well. a) and c) are porosity vs depth plots while b) and d) are pressure vs depth plots. Hydrostatic and lithostatic gradient considered 0.00105 MPa/m (0.465 psi/ft) and 0.0226 MPa/m (1 psi/ft) respectively. The reduction in pore pressure (mud weights) represented in b) and d) from the depth ~3,000 m to the end of the well ~3657 m could not be matched with the models. This reduction could be due to a change of the material conditions (e.g., natural fractures) or exposition to the surface where the pore pressure generated was dissipated. The high porosity values at ~1,000 m depth highlighted in dark blue represent the Wanstead Formation. This interval was changed to be tight for the Models_Opoutama-5T and 7T (c and d) to understand its effect.

5 Discussion

Large shallow overpressure has been encountered in the ECB during drilling and registered by pressure tests. Other overpressure manifestations such as mud volcanoes, oil and gas seeps, gas chimneys, and pock

marks have been also identified in this basin (e.g., Ridd, 1970; Plaza-Faverola et al., 2012; Erdi et al., 2018; Watson et al., 2019). However, why, and when the overpressure was generated is not properly understood yet. The primary objective of this research was to identify and quantify the main mechanisms that generated overpressure in active basins such are the ECB.

Due to the complex geological histories interpreted in the ECB, pressure estimations based on well-logs and analytical equations are not sufficient to identify the parameters and mechanisms required to generate the large overpressure values encountered at shallow depths. Therefore, geomechanical modelling was used to gain additional insights.

A regional study was performed during this research, including a geological regional assessment, seismic interpretation, well log interpretation, and 3D reservoir characterisation. However, a 1D column modelling approach was adopted here as the development of coupled forward geomechanical models capturing the evolution of a 2D section of the ECB is a complex and highly time-consuming task. Generally, capturing the structural evolution of a region in forward geomechanical models is highly sensitive to boundary conditions and material properties; in the ECB specifically, there is a large uncertainty in its geological history, structural development, and material property evolution, so that calibration of a 2D evolutionary section model is a challenging task. Nonetheless, in the present work it has been demonstrated that adopting some necessary simplifications in the modelling can provide valuable insights to pore pressure development and dissipation that are not available otherwise. As an example, the results from the parametric study have shown that for pressure prediction it is not necessary to explicitly represent all the erosional episodes, as only the effects of the recent events are relevant to the present-day overpressure. The results also shown that high levels of tectonic compression result in high pore pressure generation due to the horizontal stress generated during this process. Another important result is the impact of different sedimentation and erosion rates on porosity and pore pressure. For instance, if an X thickness is firstly eroded and later the same X thickness is deposited, the porosity and pore pressure will be lower than a sedimentary column without erosion, and it will be greater in circumstances of high sedimentation and erosion rates.

In this basin more complex models like that of Burgreen-Chan et al., (2016) were also built to investigate the evolution of pore pressure and porosity. That study was performed along a seismic section which crosses the Hawke Bay-1 well and used structural reconstructions, basin, and petroleum system models and poroelastic modelling. A key conclusion of this work was that the main overpressure mechanism was disequilibrium compaction, with less impact from tectonic compression. The conclusions of this study

differ from those of Burgreen-Chan et al., (2016), indicating that without geologically recent tectonic compression, high pore pressure values could not have been generated. Moreover, results from this study show that most of the overpressure generated by disequilibrium compaction would be dissipated due to uplift, erosion, and exhumation to the surface in some areas (e.g., Opoutama-1) and if this overpressure were retained, layers with very low permeabilities and laterally sealing faults are needed to preserve this overpressure.

Using methods similar to these, Darby and Funnell (2001) concluded that tectonic compression generated the high overpressure values in the ECB due to the subduction of the Pacific Plate under the Atlantic Plate. That study analysed pressure data to understand the distribution of the overpressure and its relationship to the subduction of the Pacific Plate underneath the Australian Plate. Darby and Funnell's (2001) work also suggests that disequilibrium compaction had an impact on present-day pore pressure due to high sedimentation rates during the Miocene (300 m/Ma), whereas the parametric models presented in this research indicate that those sedimentation rates are unlikely to cause high overpressure with the porosity-permeability curve used (Figure 4a and Figure 4b). In addition, as a result of uplift, hiatus and erosion pore pressure developed in the Miocene would largely dissipate in this basin (Figures 6e, 6g, 7a and 7b).

In the ECB several hydrocarbon seals (layers with low permeability) have been interpreted, including thick mudstone intervals (e.g., Pindari Formation) and thin low permeable limestones (e.g., Kauhauroa, Kiakia and Tahaenui limestones). However, these low permeable intervals are not present in all the wells that registered high pore pressure values. Field et al., (1997) highlighted that the marls of the Wanstead Formation were potential seals in some regions due to the large amount of smectite in such formations. In Opoutama-1 the Wanstead Formation is ~465 m thick; the effect of assigning different permeabilities on pore pressure was assessed in this research. This formation was represented in models Opoutama-7T and Opoutama-3T with high compressibility, and porosity-permeability curves with low permeabilities.

Results from model Opoutama-7T (Figures 11c and 11d) show that neither porosity, pressure nor thickness could be properly calibrated with disequilibrium compaction as the sole overpressure mechanism. Results from model Opoutama-5T (Figures 11c and 11d), which also included tectonic compression, provided a better approximation to calibration data, but there are intervals in which more adjustment needs to be done to represent the observed porosity and pore pressure trends.

6 Conclusions

In an area as geologically complex as the ECB, with multiple episodes of extension, compression and erosion, log-based analysis cannot be used to infer pore pressure or to understand pore pressure history.

Using mainly hydro-geomechanical models, this study sought to identify and quantify the mechanisms that have generated overpressure in the ECB, including assessment of sedimentation and erosion rates, thickness of eroded units, hiatus periods, low permeability intervals, and tectonic compression. Tectonic compression and disequilibrium compaction are the main overpressure mechanisms; other mechanisms such as smectite to illite, lateral transfer and hydrocarbon migration could also have contributed to pore pressure but were not considered in this study.

Strictly, 2D and 3D hydro-geomechanical models are needed to fully assess pore pressure and pore pressure histories in geologically complex regions; however, multiple uncertainties in basin reconstruction and uplift/erosion histories mean that such an approach is not practical. This study shows that 1D models are an effective tool for testing pore pressure generation hypotheses and gaining a better understanding of the influence of geological history on pore pressure evolution. Such models capture the importance of individual pore pressure generation mechanisms with a manageable array of input parameters and a practical computational timeframe. The results form the basis of 2D studies to further investigate the influence of complex stress regimes on pore pressure evolution in active tectonic basins.

Significant findings include the way in which erosion reduces pore fluid pressure due to the mechanical unloading of the overburden, leading to elastic porosity increase and the flow-driven dissipation of pore pressure during a period of erosion. Whilst erosive events are important in terms of understanding the evolution of the basin, only the latest events have an effect on pore pressure and porosity.

Furthermore, this research shows the importance of tectonic compression on pore pressure, demonstrating that the higher the horizontal compaction (12.5 %), the higher the pore pressure (model Opoutama-6T). In this model tectonic compression was applied during 2.848 Ma generating ~28 MPa more at 3,300 m depth (Figure 11b).

Even though many different parameters were investigated in multiple models in this work, pore pressure data and mud weights registered in the Opoutama-1 well still could not be totally matched by models; this could be due to the simplification of the complex geology in the 1D models, and/or the influence of the other overpressure mechanisms that were not investigated in this research.

7 Acknowledgements

This research was conducted as part of the GeoPOP4 industry supported research consortium funded by BP and Petrobras. Durham and Newcastle Universities thank these companies for funding this research.

8 References

Audet, S. M. (1996). Compaction and overpressuring in Pleistocene sediments on the Louisiana Shelf, Gulf of Mexico, *Marine and Petroleum Geology, 13*(5), 467-474.

Athy, L. F. (1930). Density, porosity, and compaction of sedimentary rocks. *AAPG Bulletin, 14*(1), 1-24.

Bailey, W. McArthur, A., McCaffrey, W. (2021). Sealing potential of contourite drifts in deep-water fold and thrust belts: Examples from the Hikurangi Margin, New Zealand, *Marine and Petroleum Geology,* 123, 1-13.

Ballance, P. F. (1975). Evolution of the Upper Cenozoic Magmatic Arc and Plate Boundary in Northern New Zealand, Earth and Planetary Science, 28, 356-370.

Ballance, P. (2017). *New Zealand Geology: an illustrated guide*. *Geoscience Society of New Zealand.* Available at: https://www.geotrips.org.nz/downloads.html#:~:text=New%20Zealand%20geology%3A%20an%20illustrated%20guide%20by%20Peter,by%20GNS%20Science%2C%20as%20stated%20in%20the%20captions. (Accessed: 03 April 2021).

Bailleul, J., Chanier, F., Ferrière, J., Robin, C., Nicol, A., Mahieux, G., Gorini, C. and Caron, V. (2013). Neogene evolution of lower trench-slope basins and wedge development in the central Hikurangi subduction margin, New Zealand, *Tectonophysics*, 591, 152-174.

Burgreen-Chan, B., Meisling, K. E. and Graham, S. (2016), Basin and petroleum system modelling of the East Coast Basin, New Zealand: a test of overpressure scenarios in a convergent margin, *Basin Research,* 28, 536-567.

Brown, B. R. (1960). Mangaone-1, Ministry of Economic Development open-file report PR320.

Butler, R. W. H. and Paton, D. A. (2010). Evaluating lateral compaction in deepwater fold and thrust belts: How much are we missing from "nature's sandbox"?, *GSA TODAY, 20*(3), 1-10.

Bruce, C. H. (1984). Smectite Dehydration – Its Relation to Structural Development and Hydrocarbon Accumulation in Northern Gulf of Mexico Basin, *AAPG Bulletin,* 68, 673-683.

Couzens-Schultz, B. A., & Azbel, K. (2014). Predicting pore pressure in active fold-thrust systems: An empirical model for the deepwater Sabah foldbelt. *Journal of Structural Geology* 69, 465-480.

Dalton, T. J. S. Paton, D. A., Needham, T. and Hodgson, N. (2015). Temporal and spatial evolution of deepwater fold thrust belts: Implications for quantifying strain imbalance Interpretation, G*eoScienceWorld, 3*(4), 59-70.

Darby, D. and Ellis, S. (2001). Evaluating overpressure in Compressional Regimes using Geomechanical Modelling, *Petroleum Exploration society of Australia,* 613-620.

Darby, D. and Funnell, R. H. (2001). Overpressure associated with a convergent plate margin: East Coast Basin, New Zealand. *Petroleum Geoscience,* 7, 291-299.

Erdi, A., Huuse, M. and Bachtiar, A. (2018). Tectonic Evolution and Hydrocarbon Prospectively of East Coast Basin, Offshore Hawke Bay, New Zealand, *Offshore Technology Conference,* 1-18.

Field, B. D., Uruski, C. I. and others (1997). Cretaceous-Cenozoic Geology and Petroleum System of the East Coast Region, New Zealand. *Institute of Geological and Nuclear Sciences monograph 19*, 301.

Funnell, R., Chapman D., Allis, R. and Armstrong, P. (1996). Thermal state of the Taranaki Basin, New Zealand, *Journal of Geophysical Research*, 101,197-215.

Funnell, R., H, R., Wood, R. A., Stagpoole, V. M, Uruski, C., Scadden, P., Killops, S. d., Cutress, G., Field, B. D. and Nicol, A. (1999). Thermal and hydrocarbon generation modelling of Hawke Bay area (PEP38325, 38326, 38329), Ministry of Economic Development open-file report PR4311.

GEBCO Gridded Bathymetry Data. (Available at: https://www.gebco.net/data_and_products/gridded_bathymetry_data/ .(Accessed; 05 May 2021).

GNS New Zealand Crown Research Institute. Available at: Home - GNS Science . (Accessed; 20 November 2020).

Hansen, S. (1996). A compaction trend for Cretaceous and Tertiary shales on the Norwegian Shelf based on sonic transit times. *Petroleum Geoscience,* 2, 159-166.

Hantschel, T., & Kauerauf, A. I. (2009). *Fundamentals of basin and petroleum systems modeling.* Aachen, Germany: Springer.

Haskell, T. R. (2005). Development of Definition of Petroleum System used in Exploration Work in the East Coast Basin, New Zealand, Ministry of Economic Development open-file report PR3178.

J. A. R. (1985). East Coast Oil Exploration Ltd. NZ, New Zealand, Ministry of Economic Development open-file report PR1086.

Lillie, A. R. (1953). The Geology of the Dannevirke Subdivision, *New Zealand Geological Survey,* 46, 1-153.

Martin, K. R. (1995). Petrology of reservoir formations in PPL 38316 and PPP 38324, Western and Northern Hawkes Bay, East Coast Basin, New Zealand, Ministry of Economic Development open-file report PR2556.

Neef, G. (1992). Turbidite deposition in five Miocene bathyal formations along an active plate margin, North Island, New Zealand: with notes on styles of deposition at the margins of the east coast bathyal basins, *Sedimentary Geology,* 78, 111-136.

Nicol, A., VanDissen, R., Vella, P., Alloway, B. and Melhuish, A. (2002). Growth of contractional structures during the last 10 m.y. at the southern end of the emergent Hikurangi forearc basin, New Zealand, *New Zealand Journal of Geology and Geophysics, 45*(3), 365-385.

NZ Aquitaine Petroleum Ltd. (1967). Opoutama-1 well report, Ministry of Economic Development open-file report PR504.

NZPAM New Zealand Petroleum and Mine Online Exploration Database. Available at: https://data.nzpam.govt.nz/GOLD/system/mainframe.asp . (Accessed; 05 October 2020).

Obradors-Prats, J., Rouainia, M., Aplin, A. C., & Crook, A. J. L. (2017a). Assessing the implications of tectonic compaction on pore pressure using a coupled geomechanical approach. *Marine and Petroleum Geology,* 79, 31-43.

Obradors-Prats, J., Rouainia, M., Aplin, A. C., and Crook, A. J. L. (2017b). Hydromechanical modeling of stress, pore pressure, and porosity evolution in fold-and-thrust belt systems. *Journal of Geophysical Research: Solid Earth, 122*(11), 9383-9403.

Parageo. Available at: www.parageo.co.uk

Petrel. Available at: www.software.slb.com/products/petrel

Petromod. Available at: www.software.slb.com/products/petromod

Plaza-Faverola, A., Klaeschen, D., Barnes, P., Pecher, I., Henrys, S. and Mountjoy, J. (2012). Evolution of fluid expulsion and concentrated hydrate zones across the southern Hikurangi subduction margin, New Zealand: An analysis from depth migrated seismic data, *Geochemistry, Geophysics, Geosystems,* 13, 1-21.

Raine, J. I., Beu, A. G., Boyes, A. F., Campbell, H. J., Cooper, R. A., Crampton, J. S., Crundwell, M. P., Hollis, C. J., Morgan, H. E. G. and Mortimer, N. (2015). New Zealand Geological Timescale NZGT, New Zealand Journal of Geology and Geophysics, 58(4), 398-403.

Reyners, M. (2013). The central role of the Hikurangi Plateau in the Cenozoic tectonics of the New Zealand and the Southwest Pacific, *Earth and Planetary Science Letters,* 361, 460-468.

Ridd, M. F. (1970). Mud Volcanoes in New Zealand, *The American Association of Petroleum Geologist Bulletin,* 54, 601-616.

Rogers, K. M., Collen, J. D., Johnston, J. H., and Elgar, N. E. (1999). A geochemical appraisal of oi seeps from the East Coast Basin, New Zealand, *Organic Geochemistry*, 30, 593-605.

Tingay, M. R. P., Hillis, R. R., Swarbrick, R. E., Morley, C. K. and Damit, A. R. (2009). Origin of overpressure and pore-pressure prediction in the Baram province, Brunei. *AAPG Bulletin,* 93, 51-74.

Schneider, F. Potdevin, J. L., Wolf, S., and Faille, I. (1996). Mechanical and chemical compaction models for sedimentary basin simulators, *Tectonophysics,* 263, 307-317.

Simpson, Jeremy and Jarvis, J. (1993). Technical review of the East Coast Basin, New Zealand, Ministry of Economic Development open-file report PR1972.

Swarbrick, R. E. and Hillis, R. R. (1999). The Origin and Influence of Overpressure with Reference to the North West Shelf, Australia, *The APPEA Journal*, 39, 64-72.

Swarbrick, R. E., Osborne, M. O. and Yardley, G. S. (2002). Comparison of Overpressure Magnitude Resulting from the Main Generating Mechanisms, in Huffman, A. R. and Bowers, G. L. (eds.) *Pressure regimes in sedimentary basins and their prediction.* AAPG Memoir 76, 1-12.

Watters, W. A. (1990). Petrography and Diagenesis of Rocks from Coastal Wairarapa, adjacent to PPL38318 and 38323 East Coast Belt, New Zealand, Ministry of Economic Development open-file report PR1585.

Watson, J. F. (1962). Ruakituri-1, Ministry of Economic Development open-file report PR324.

Watson, S. J., Mountjoy, J. J., Barnes, P. M., Crutchley, G. J., Lamarche, G., Higgs, B. Hillman, J., Orpin, A. R., Micallef, A., Neil, H., Mitchell, J., Pallentin, A., Kane, T., Woelz, S., Bowden, D., Rowden, A. A. and Pecher, I. A. (2019). Focused fluid seepage related to variations in accretionary wedge structure, Hikurangi margin, New Zealand, *The Geological Society of America*, 48, 56-61.

Wyllie, M. R. J., Gregory, A. R. & Gardner, L. W. (1956). Elastic wave velocities in heterogeneous and porous media. *Geophysics*, 21, 41-70.